Slope Stability 2007 — Y. Potvin (ed)

https://papers.acg.uwa.edu.au/p/708_18_Sainsbury/

Three-Dimensional Discontinuum Analysis of Structurally Controlled Failure Mechanisms at the Cadia Hill Open Pit

D. Sainsbury *Itasca Australia Pty Ltd, Australia*

F. Pothitos *Ok Tedi Mining Ltd, Papua New Guinea (formerly Newcrest Mining Ltd, Australia)*

D. Finn *Newcrest Mining Ltd, Australia*

R. Silva *Itasca S.A., Chile*

Abstract

The south wall of Newcrest Mining Ltd's Cadia Hill Open Pit experienced a multi-bench (60,000 t) failure during 2006. The observed failure mechanism is a combination of structurally controlled and rock mass failure. The 3DEC code has been developed by Itasca specifically to study complex failure mechanisms involving large numbers of explicit structures (joints, faults) that divide a rock mass into blocks. Slip, separation and rotation along explicit structures can occur, while the individual blocks can also deform and yield.

The following paper details a series of analyses that have been conducted with 3DEC to back-analyse the observed behaviour of the south wall, which happened when mining was at the 505 RL level. The calibrated model has subsequently been used to investigate the behaviour of the south wall after mining has progressed down to the 445 RL level.

1 Introduction

Newcrest Mining Ltd's Cadia Hill Open Pit Mine, near Orange in New South Wales, is located within a complex geological setting. The current pit-slope design is based upon structurally controlled failure mechanisms associated with faults and shear zones that dissect a largely massive rock mass. To date, a number of structurally controlled slope failures have occurred along fault and shear planes with minimal warning. Their scales have ranged from less than one bench height to multiple bench heights.

Routine kinematic, limit equilibrium and two-dimensional numerical modelling analyses are an essential part of any pit-slope design methodology. However, in order to determine accurately the stability of complex wedge-failure mechanisms that involve a combination of rock mass failure in addition to slip along geological structure, a three-dimensional discontinuum analysis is required.

2 Background

Mining commenced at the Cadia Hill Pit during 1997. Figure 1a illustrates Cutback 2, which forms the current pit shell that is being mined. The pit currently measures 1.5 km across, with slope heights ranging from 330 to 490 m. The inter-ramp slope angles range from 35° for the top 100 m in weathered sediments, to 55° for the bottom 135 m of the cutback. The final pit, as illustrated in Figure 1a, currently is designed to be 580 to 720 m deep (Li, 2005).

Following the firing of a trim shot on 9 September 2006, approximately 60,000 t of rock failed in the centre of the south wall from 535 - 656 RL, as illustrated in Figure 1b. There had been 5 mm of rainfall recorded on the day before the failure, and intermittent light rain had occurred during the day of the failure.

A large-scale (trace length > 30 m) shear structure, running sub-parallel to the face at an orientation of 56°/004° formed a basal sliding plane for the failure, as illustrated in Figure 1c. The failure occurred within geological Domain 18, which is comprised of monzonite. The rock mass in this domain is characterised by moderate-to-high RQD values and high intact rock strength (Finn, 2006).

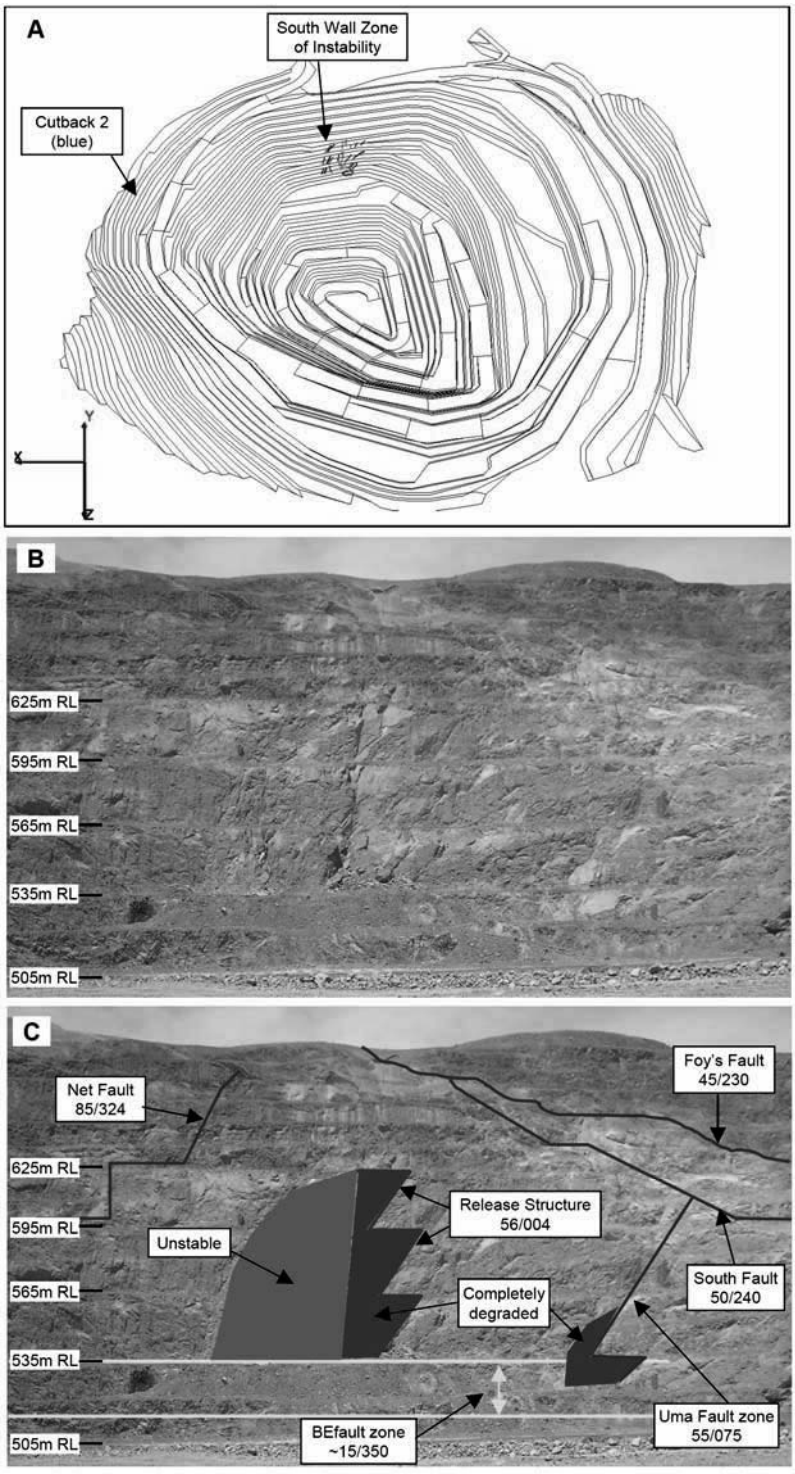

Figure 1 View of the Cadia Hill pit south wall (looking south)

Slope monitoring in the form of survey prisms and radar has been conducted since the beginning of 2006. Prism monitoring identified acceleration in slope displacements during May-June 2006, coincident with mining of the 550 RL level. Increases in slope movements have also been observed to be coincident with blasting and rainfall events.

The south wall failure was a combination of structurally controlled and rock mass failure. The release structure does not form a daylighting wedge that can be analysed using traditional wedge-failure analysis techniques. A conceptual model of the failure mechanism is illustrated in Figure 2, whereby sliding along the shear structure is combined with tensile and shear failure of the rock mass to cause the observed slope failure.

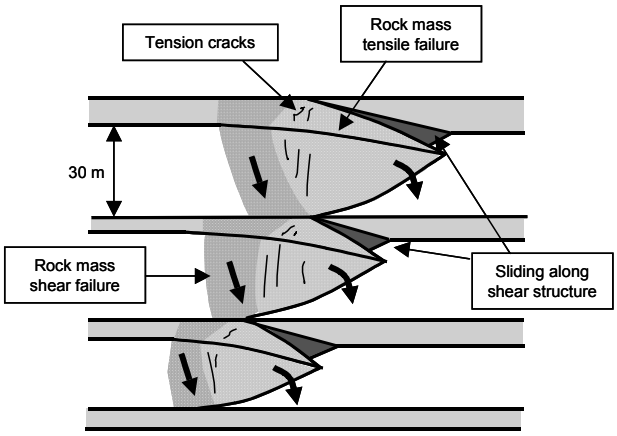

Figure 2 Conceptual model of south wall failure mechanism

Routine two-dimensional limit equilibrium analyses have been conducted for slope design and back-analysis of the multi-bench failure. However, due to the complex nature of the failure mechanism, these traditional methods of pit slope stability analysis have been unable to back-analyse the observed behaviour of the south wall instability.

3 Geotechnical model

The south wall geotechnical model developed for the initial slope design was largely based upon drill hole information with little pit wall exposure data to calibrate the structural model. To manage this uncertainty a large step-in was designed at the 505 RL level. Additional drilling was conducted during late 2005. This additional data was used in conjunction with bench face mapping in order to update the geotechnical model during 2006.

3.1 Geology

The predominant lithology throughout the south wall is monzonite Volcanics and Silurian sediments are also present, associated with faulting.

3.2 Structural geology

The Cadia Hill pit is located on the footwall of several thrust structures. There have been approximately four structural deformation episodes that have contributed to structures having a curvilinear nature, short persistence and varying mechanical properties along the length of the structure. Figure 3 illustrates the structures identified within the 2006 structural model.

Estimates of the shear strength parameters for each south wall structure have been made using field measurements of joint roughness coefficient (JRC) and joint wall compressive strength (JCS). Table 1 presents estimates of the orientation, thickness and shear strength properties for each structure.

Table 1 Estimates of the shear strength parameters for each south wall fault structure

Structure	Dip (deg).	Dip Dir. (deg.)	Thickness (m)	Cohesion (kPa)	Fric. Angle (deg.)
Foy's Fault	45	230	1.0	20	20
South Fault	50	240	0.2	20	25
Net Fault	85	324	0.1	20	25
Uma Fault Zone	55	75	1.0	50	25
BE Fault Zone	15	330	20.0	0	20

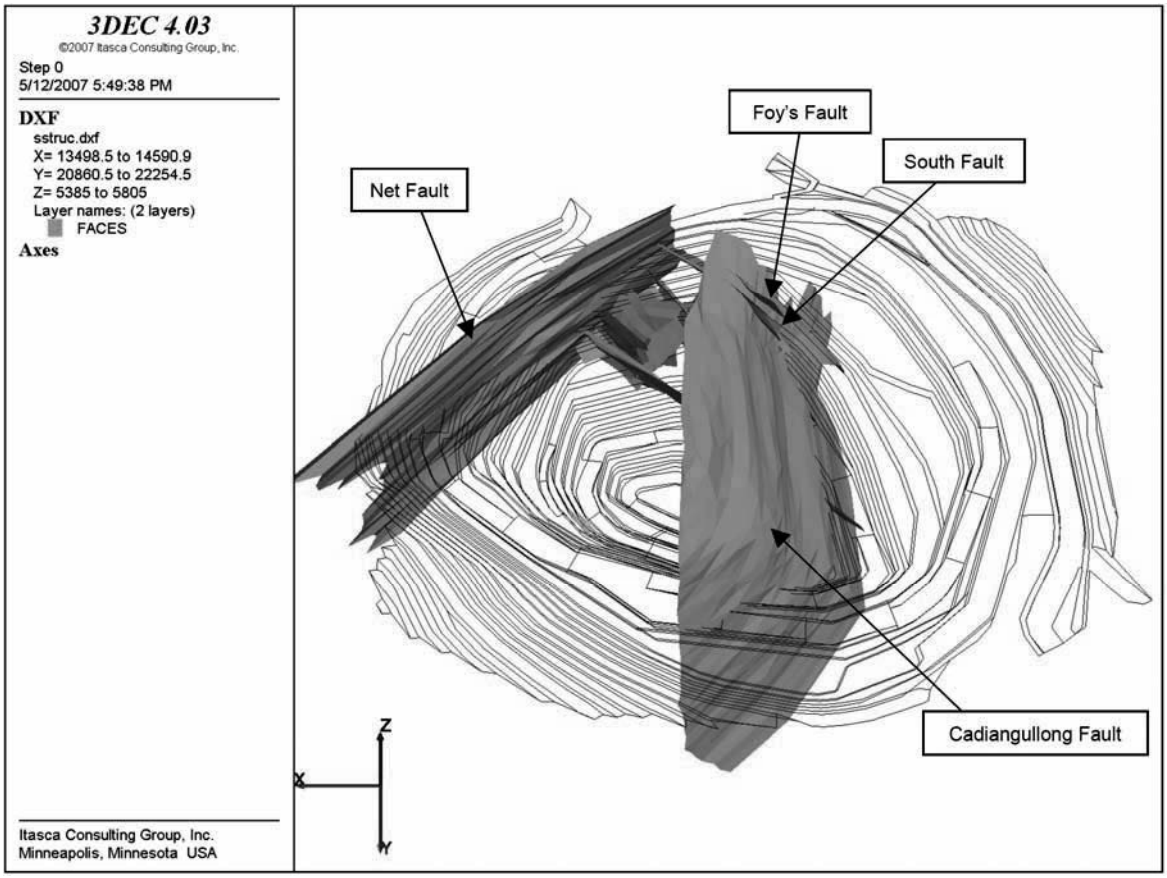

Figure 3 2006 structural model (looking south)

3.3 Rock mass characterisation

The south wall failure occured within monzonite. Laboratory testing of intact samples of this material indicates an unconfined compressive strength (UCS) of 120 MPa. Drillhole and bench face mapping has been conducted to determine the GSI rating for Domain 18. Table 2 presents the rock mass parameters determined for Domain 18 and the BE Fault Zone.

Table 2 Rock mass parameters

Domain/Unit	GSI	σ^{ci} (MPa)	m^i
Domain 18	60–75	120	21
BE Fault Zone	50–60	100	21

For slope stability analysis purposes, it is important to understand that the GSI rating derived at the bench-slope scale needs to be degraded to account for the analysis of inter-ramp and overall pit slopes. This scale-effect phenomenon has been reported by several authors to have a significant impact on rock mass strength, as illustrated in Figure 4. Pothitos (2005) applied a nominal reduction factor of 0.8 to the GSI for analysis of 200 m slopes at the Cadia Hill Pit.

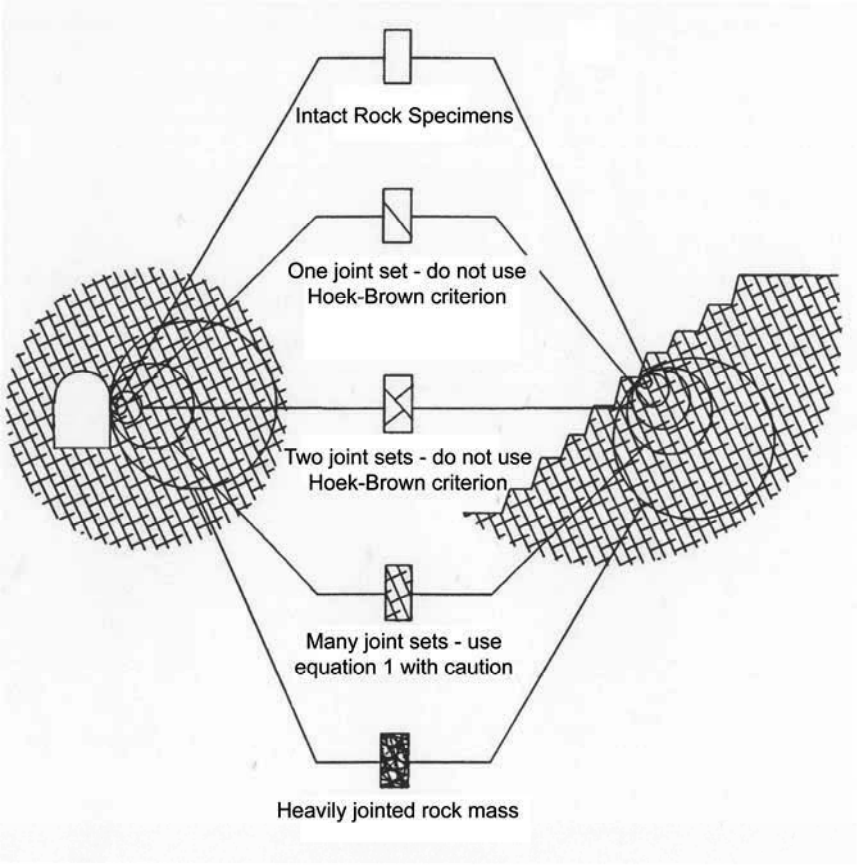

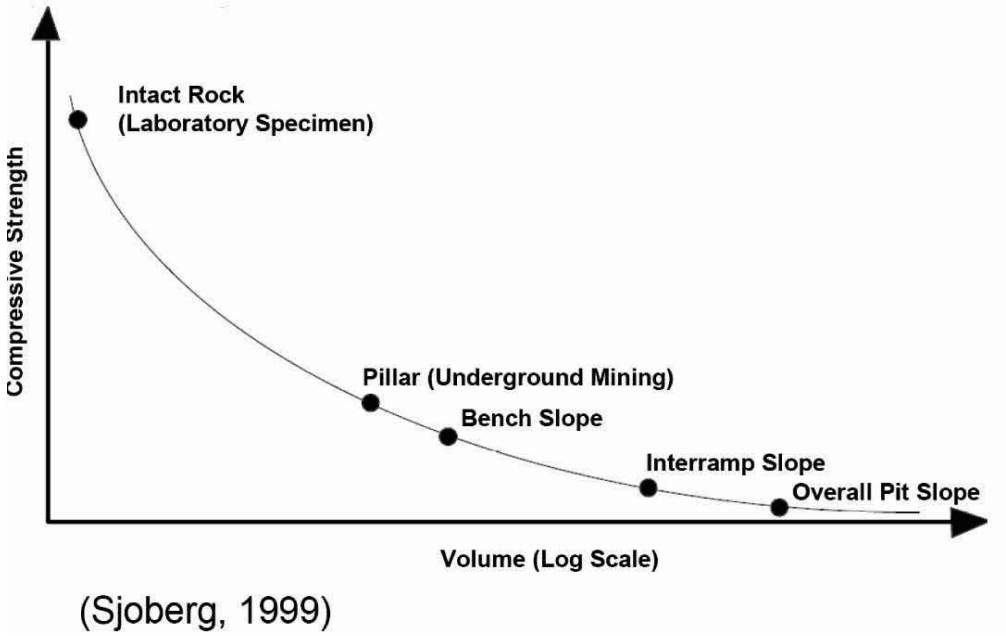

Figure 4 Rock mass scale effects (after Hoek et al., 1995 and Sjöberg, 1999)

3.4 Hydrogeology

Two vibrating-wire piezometers are located along the crest of the south wall. The phreatic surface interpreted is illustrated in Figure 5. Both piezometers show no reaction to rainfall events. Water seepage has been evident along the south wall at several levels. Along the 610 RL level, several drainholes produced flow rates of approximately 2 l/s.

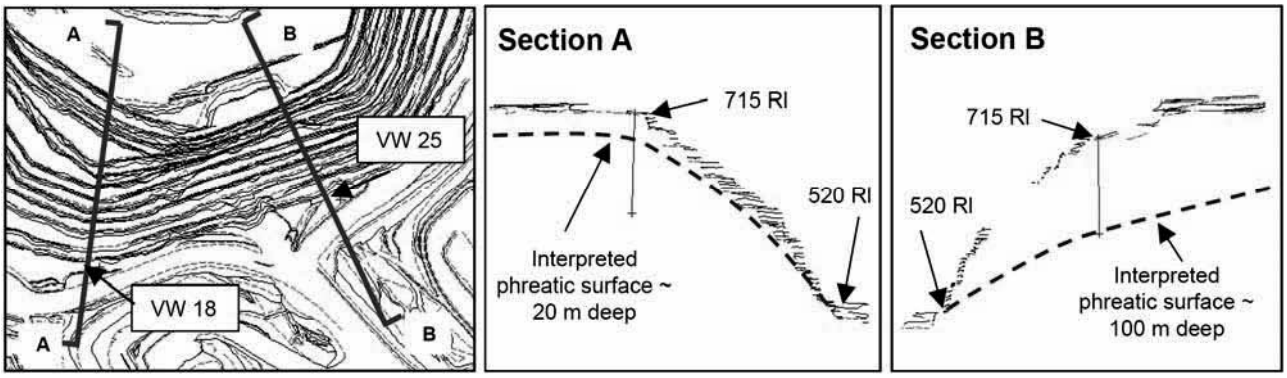

Figure 5 Estimated phreatic surface based upon vibrating wire piezometers

4 Numerical analysis of the Cadia Hill pit south wall

The *3DEC* code (Itasca, 2007) has been developed specifically to study complex failure mechanisms involving large numbers of explicit structures that divide a rock mass into blocks. Slip, separation and rotation along explicit structures can occur, while the individual blocks can deform and yield.

4.1 Model geometry

Figure 6 illustrates the *3DEC* model constructed to simulate the south wall of the Cadia Hill Pit. For the purpose of initial model calibration and investigation of the behaviour of the south wall in the vicinity of the failure, only the south wall to an elevation of 445 RL was constructed. Due to the orientation of the model, displacements at the boundaries were fixed. This limits interpretation of model behaviour close to the boundaries.

The large-scale structures included within the *3DEC* model are illustrated in Figure 6. The BE Fault Zone has been represented as a 20 m thick zone of weaker material bounded by discrete, planar joint surfaces. All other structures have been simplified as discrete planar surfaces.

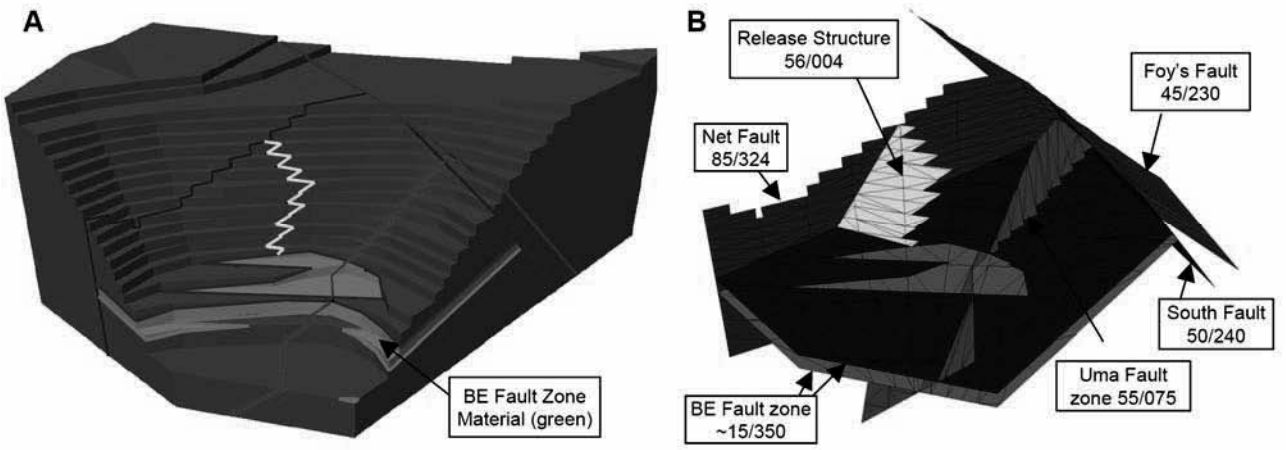

Figure 6 Large-scale structures included within *3DEC* model

4.2 Modelling methodology

A bi-linear Mohr-Coulomb strain-softening constitutive model was used to represent the behaviour of the rock mass. Because the Mohr-Coulomb criterion was used to define the strength of the rock mass, values for cohesion and friction angle were obtained by a least-squares fit to the Hoek-Brown curve. A bi-linear fit was obtained over a range in confining stress from 0 to 1 MPa and 1 to 5 MPa. An example of a bi-linear curve for a material with a GSI of 50, σ_{ci} of 120 MPa and m_i of 21 is illustrated in Figure 7.

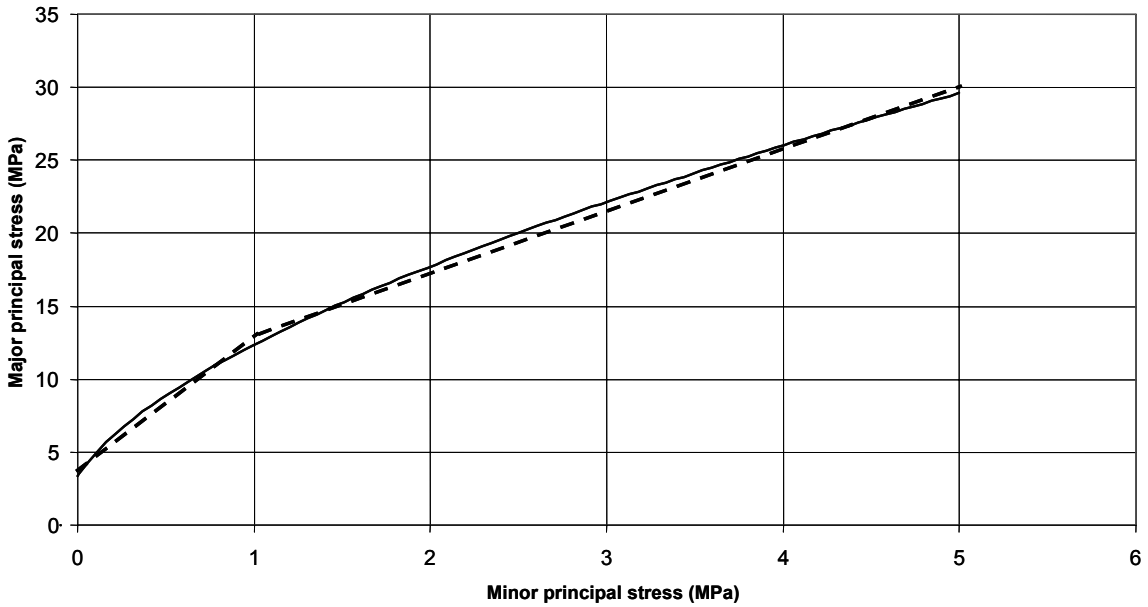

Figure 7 Relation between major and minor principal stresses for Hoek-Brown (solid line) and equivalent bi-linear Mohr-Coulomb (dashed line)

The specification of ductile or brittle behaviour in a numerical model is a very important consideration, as brittle materials tend to undergo progressive collapse much sooner after yielding begins. Ductile materials, on the other hand, are likely to remain stable well after yielding begins. For this reason, a strain-softening model has been used to represent the post-peak strength degradation that accompanies failure of the south wall rock mass.

Sjöberg (1999) states that strain-softening model results are dependent on the model grid used and recommends that strain-softening models should not be used for quantitative rock-slope stability analysis. However, advances in the understanding of strain-softening mesh dependency (Sainsbury and Urie, 2007), together with calibration of the strain-softening parameters to observed slope behaviour allows the use of such models in routine rock-slope stability analysis. Hajiabdolmajid and Kaiser (2002) suggest that a strain-softening material model must be used to simulate accurately the behaviour of rock slopes in which the candidate failure surface is not completely structurally controlled (i.e. failure of intact rock, asperities and rock bridges are involved).

Figure 8 illustrates the results of a simulated *3DEC* UCS test on a 10 × 10 × 10 m rock mass sample with a GSI of 50, σ_{ci} of 120 MPa, m_i of 21 and D of 1.0. The modelling methodology causes localization along shear bands whereby the cohesion and tensile strength have degraded from the intact value to zero. This is the same behaviour observed in physical UCS tests. The strength of the rock mass was degraded by means of gradual reductions in the cohesion and tensile strength with plastic strain (ε^s_{crit}). The cohesion and tensile strength parameters were reduced to zero.

There is currently no a priori way to estimate the value for the critical plastic strain of a rock mass. In order to provide a more robust assessment of the rock mass strength, modulus, brittleness and scale effect of the different rock mass domains at the Cadia Hill Pit, it is planned to investigate rock mass behaviour with the Particle Flow Code (PFC) (Itasca, 2005).

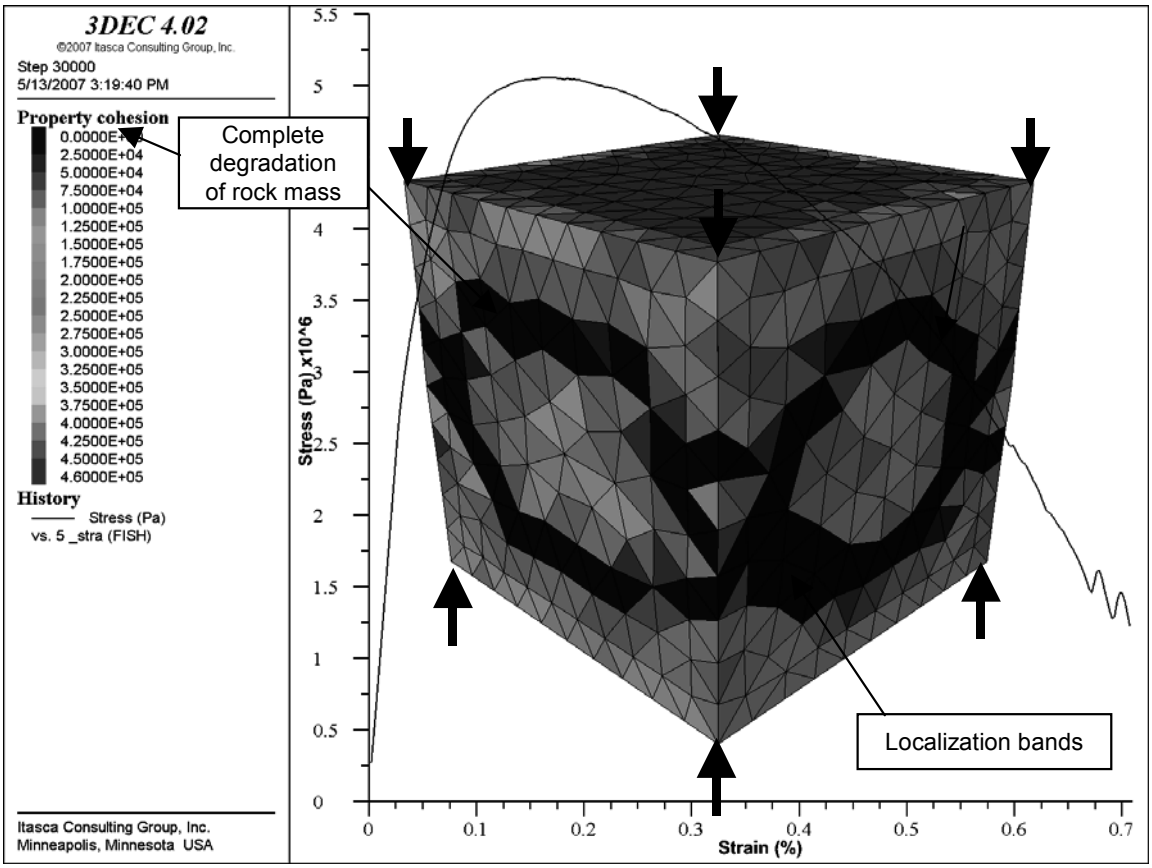

Figure 8 Simulated UCS test on 10-m rock mass sample with GSI of 50, σ_{mi} of 120 and m_i of 21

4.3 Material properties

The rock masses simulated throughout this modelling exercise are assumed to behave as a homogeneous, isotropic material. Table 3 outlines the estimates of the material properties used to simulate the south wall rock mass.

Table 3 Estimates of Mohr-Coulomb parameters for the south wall rock mass

Class	σ_{ci} (MPa)	GSI	m_i	D	Density (kg/m^3)	Young's Modulus (GPa)	Poisson's ratio	Cohe-sion (MPa)	Friction Angle (deg.)	Cohe-sion (MPa)	Friction Angle (deg.)	Tension (kPa)
								σ_3 = 0-1 (MPa)		σ_3 = 1-5 (MPa)		
Lower bound	120	50	21	1.0	2700	4.9	0.25	0.46	50	1.26	37	50
Best estimate	120	57.5	21	1.0	2700	9.0	0.25	0.63	54	1.55	41	100
Upper bound	120	70	21	1.0	2700	15.8	0.24	1.27	59	2.36	48	320

The rock mass material within the BE Fault Zone was simulated with separate material properties. Table 4 presents lower-bound and best-estimate properties used to simulate the BE Fault Zone rock mass.

Table 4 Estimates of Mohr-Coulomb parameters for the BE fault zone rock mass

Class	σ_{ci} (MPa)	GSI	m_i	D	Density (kg/m^3)	Young's Modulus (GPa)	Poisson's ratio	Cohesion (MPa)	Friction Angle (deg.)	Cohesion (MPa)	Friction Angle (deg.)	Tension (kPa)
								σ_3 = 0-1 (MPa)		σ_3 = 1-5 (MPa)		
Lower bound	100	40	21	1.0	2700	5.0#	0.25#	0.30	41	0.88	29	16
Best estimate	100	50	21	1.0	2700	5.0	0.25	0.43	48	1.18	35	41

The Mohr-Coulomb parameters used to simulate each fault structure are presented in Table 5.

Table 5 Estimates of Mohr-Coulomb parameters for fault structures

Class	Fault	Normal stiffness (Pa/m)	Shear stiffness (Pa/m)	Cohesion (kPa)	Friction Angle (deg).	Tension (kPa)
Best estimate	Foy's	1.00E+10	1.00E+09	20	20	0
Best estimate	Net	1.00E+10	1.00E+09	20	25	0
Best estimate	Uma	1.00E+10	1.00E+09	20	25	0
Best estimate	South	1.00E+10	1.00E+09	50	25	0
Best estimate	BE	1.00E+10	1.00E+09	0	20	0

4.4 Pre-mining stresses

A series of HI Cell and acoustic emission (AE) stress measurements have been taken underground at the nearby Ridgeway Mine. Based upon these measurements, the vertical stress at the Cadia Hill Pit was assumed to be lithostatic (assuming a density of 2700 kg/m^3). The pre-mining stresses used throughout the analyses are summarised in Table 6.

Table 6 Pre-mining stresses used in analyses

Principal stress	Stress-depth relation (MPa)	Orientation
σ_v	Overburden (2700 kg/m^3)	Vertical
σ_H	1.72 x σ_v	East-west
σ_h	1.25 x σ_v	North-south

5 Calibration of south wall failure after mining of the 505 RL bench

In order to calibrate the *3DEC* model to the observed behaviour of the south wall failure after mining of the 505 RL bench, a series of analyses was conducted whereby the upper-bound (GSI = 70), best-estimate (GSI = 57.5) and lower-bound (GSI = 50) rock mass properties were simulated. The best-estimate properties for the BE Fault zone (GSI = 50) were simulated, while best-estimate joint properties and phreatic surface conditions also were applied to the models.

The south wall failure mechanism observed throughout the modelling exercise is illustrated in Figure 9. Sliding along the non-daylighting release structure, combined with tensile failure of the rock mass, causes the observed multi-bench slope failure.

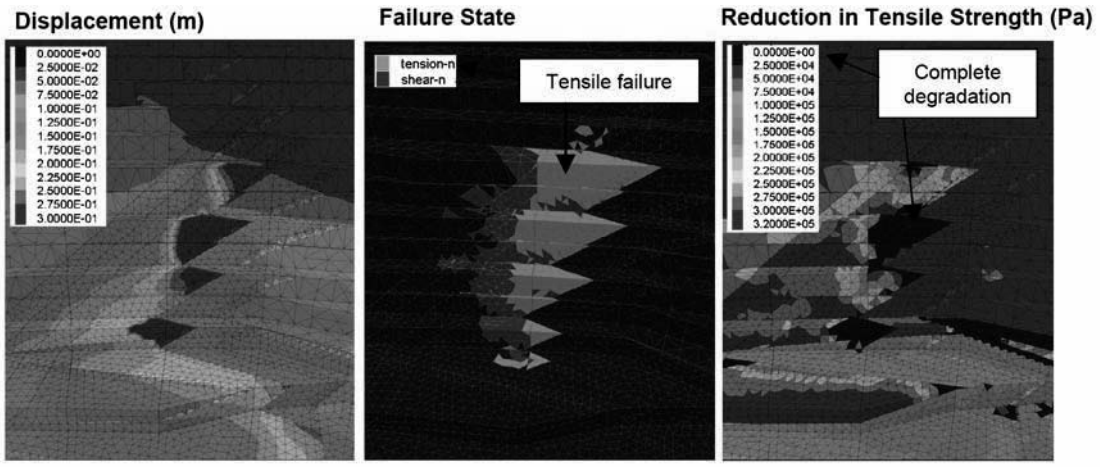

Figure 9 Failure mechanism predicted with *3DEC*

The best-estimate rock mass properties, with a GSI of 57.5, provide a good calibration to the observed behaviour of the south wall failure. Figure 10 illustrates a comparison between the observed and predicted conditions of the south wall after mining of the 505 RL bench. Together with the main multi-bench failure, the bench-scale failure associated with the Uma Fault zone is also predicted within the *3DEC* model.

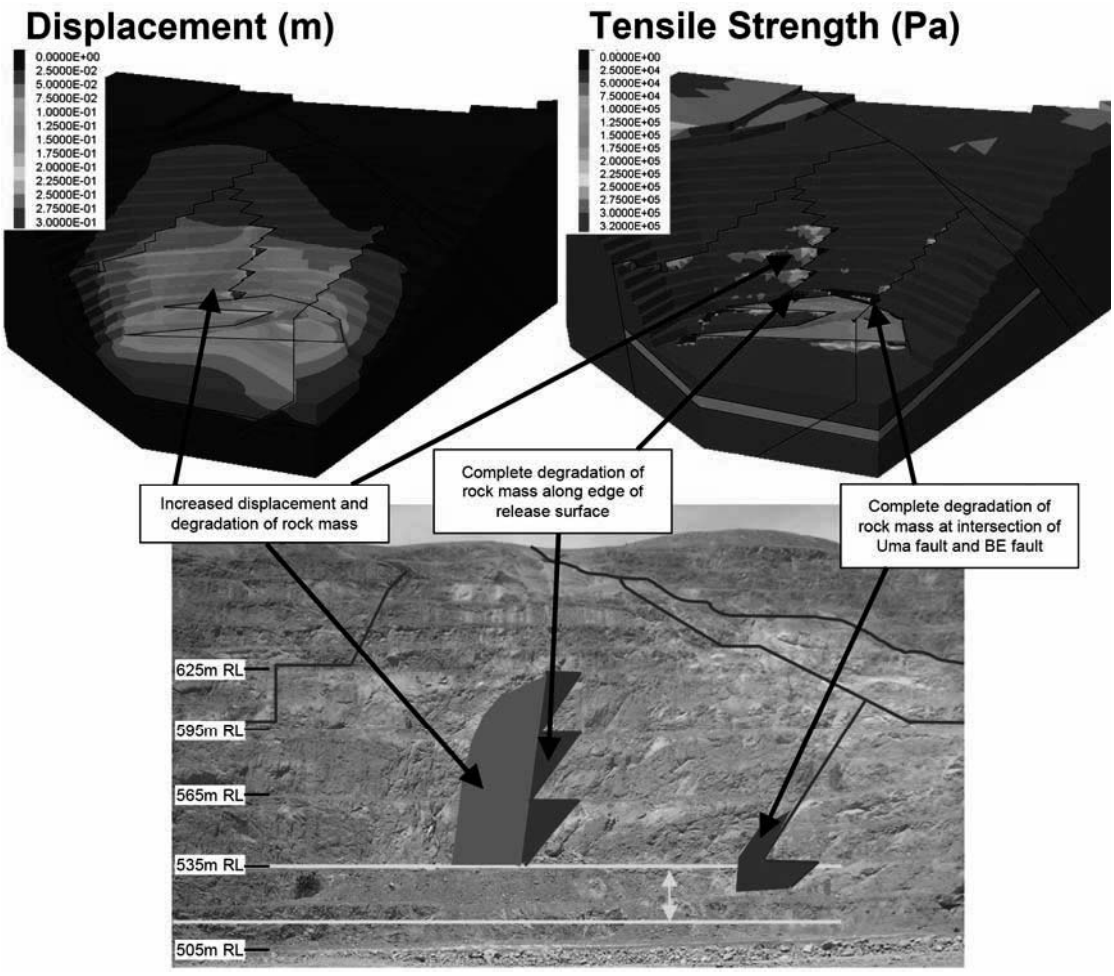

Figure 10 Comparison of observed and predicted behaviour of south wall with a GSI of 57.5

Histories of slope displacements have been measured at the same locations as monitoring prisms with the *3DEC* model. A comparison between the measured and predicted slope displacements is illustrated in Figure 11. Because real time is not simulated within the numerical model, the model displacements have been scaled to the excavation sequence of the south wall. A good correlation has been obtained between the measured and predicted slope displacements.

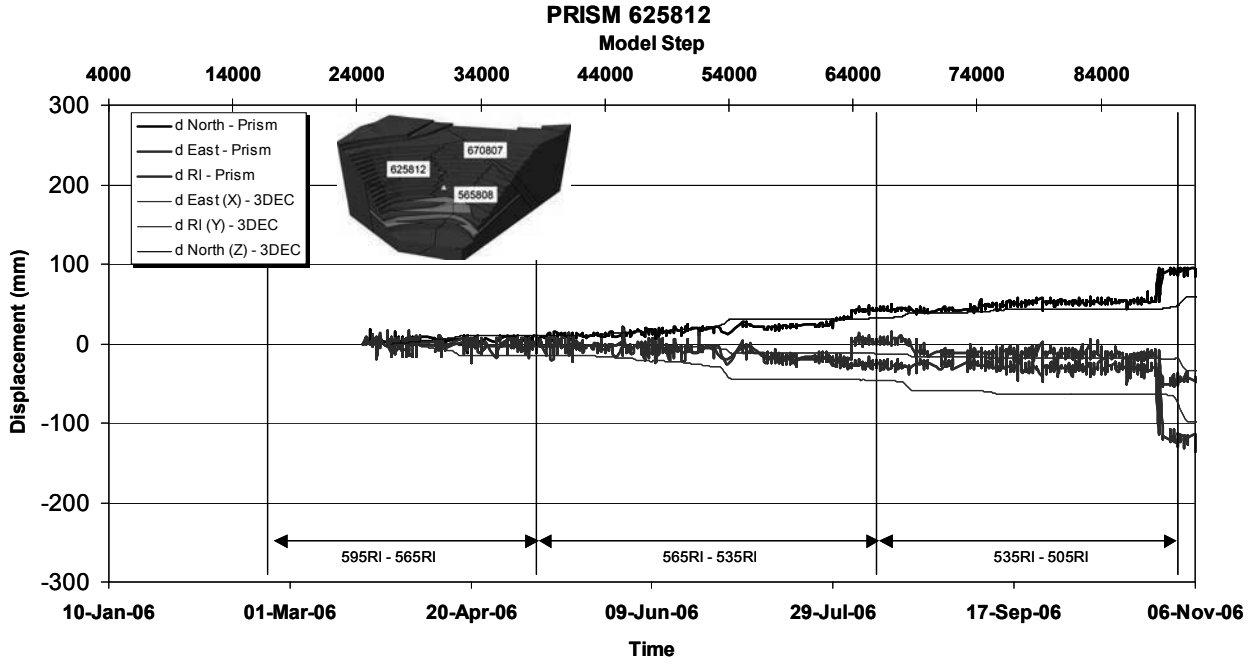

Figure 11 Comparison of actual and predicted slope displacement at prism 625812 location

6 Analysis of south wall behaviour after mining of 445 RL Bench

Due to the good calibration with the observed behaviour of the south wall failure, the best-estimate (GSI = 57.5) rock mass model was used to investigate the likely behaviour of the south wall after mining of the 445 RL bench. Figure 12 illustrates the slope displacement and reduction in tensile strength in the area of the failure. A minor increase in displacement and yielding is observed, but the vertical extent of the failure zone is predicted to remain confined to an approximate 60 m width between 625 RL and 535 RL, bounded by the original release structure.

Figure 13 illustrates the predicted slope displacements as mining progresses from the 505 RL bench to the RL bench. The 625812 prism location is predicted to become unstable during mining between the 475 RL and 445 RL benches.

7 Analysis of 475 RL bench failure

On 23 March 2007, a 35,000 to 40,000 t failure occurred on the 475 RL bench face, in the southwest corner of the Cadia Hill Pit. The failure was triggered by significant rainfall immediately before the time of failure.

Inspection of the failure, reported by Lowther (2007), identified a shallow-dipping shear structure (25º/082º) associated with the BE Fault zone that formed the basal plane of the failure. The failed volume of rock was observed to be intensely jointed.

Although the *3DEC* models analysed do not account for the pore pressures and increased rock-mass density caused by significant rainfall surface runoff, as illustrated in Figure 14, the best-estimate rock mass model indicates a zone of increased displacement and yielding associated with the BE Fault zone on the 475 RL bench face, in the exact location as the observed failure. Analysis of the 475 RL bench failure highlights how a *3DEC* modelling approach can be used as a predictive tool to identify problem areas within the mining sequence.

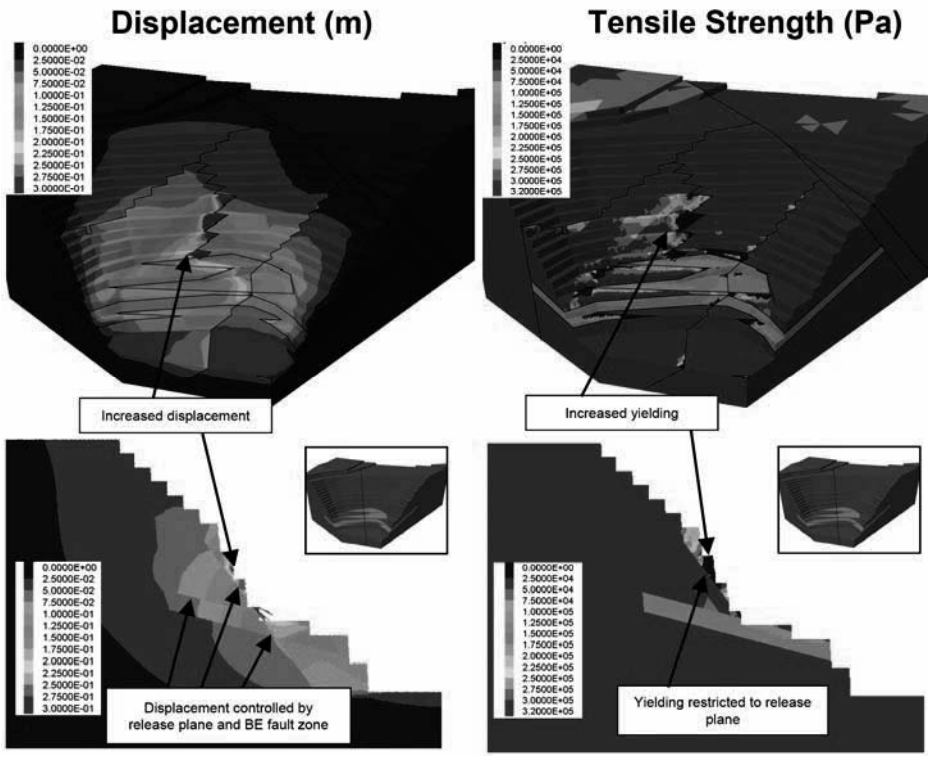

Figure 12 Displacement and reduction in tensile strength after mining of 445 RL bench

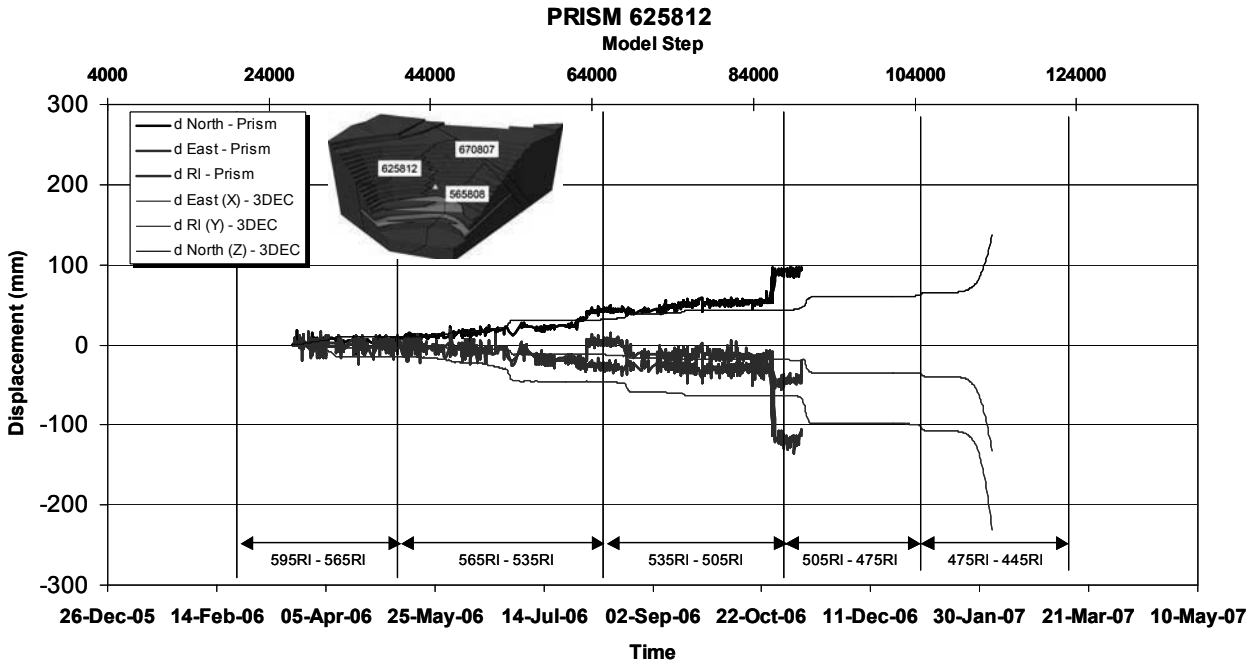

Figure 13 Comparison of actual and predicted slope displacement at prism 625812 location after mining of 445 RL bench

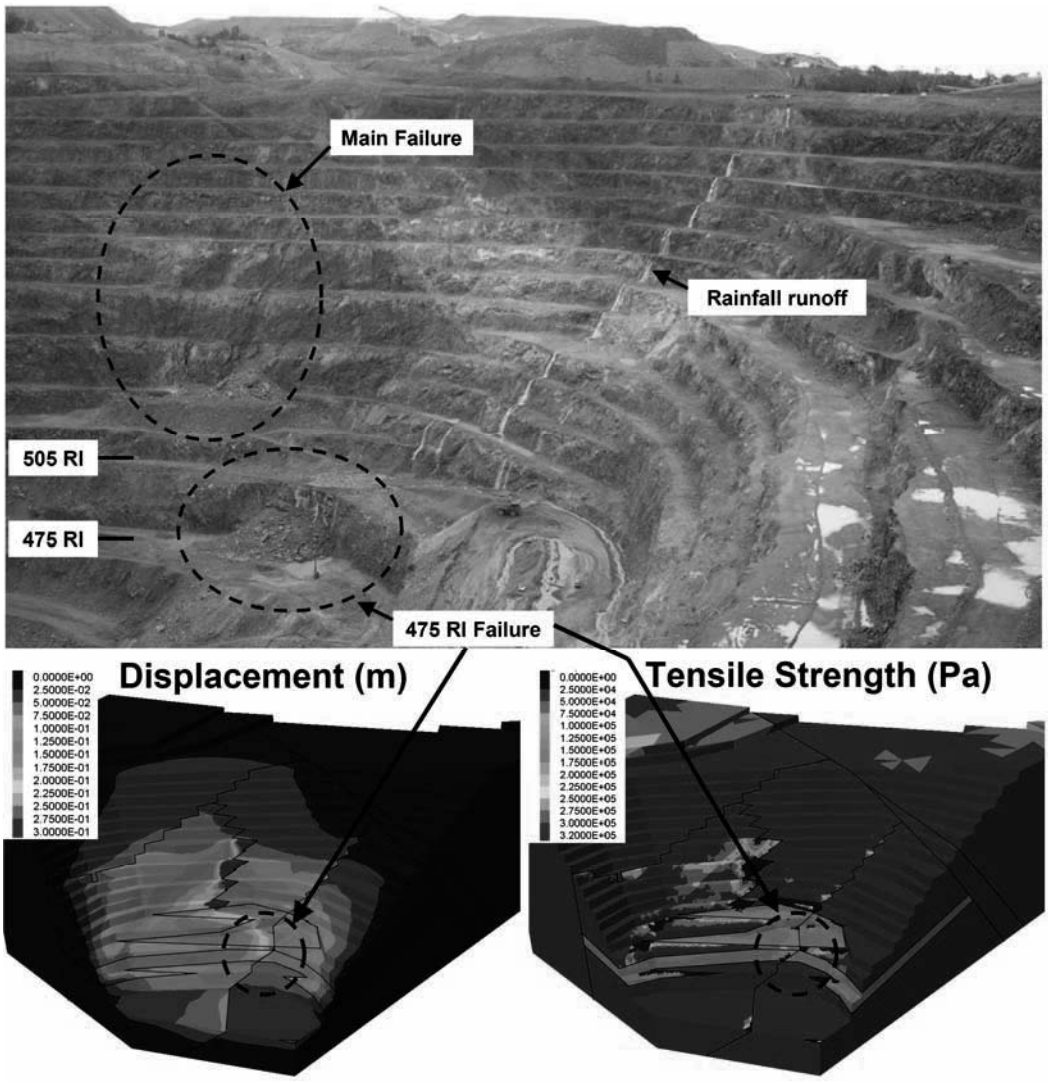

Figure 14 Analysis of 475 RL bench failure

8 Discussion of uncertainties and limitations

In order to understand the sensitivity of the south wall slope behaviour to the different model parameters, a series of analyses was conducted whereby the structure properties, phreatic surface, BE Fault zone material strength and slope angle were varied independently over reasonable upper and lower bound ranges. A single analysis was also conducted in order to investigate the combined effect of the lower-bound model parameters. The combined worst case slope conditions have a significant effect upon the extent of the south wall failure, whereby failure is predicted to propagate to the west, terminating at the Net Fault, as illustrated in Figure 15. Based upon calibration of the observed south wall failure after mining to the 505 RL bench, this condition clearly represents an overly conservative analysis of the slope behaviour.

Analysis of pit slope behaviour with a *3DEC* modelling approach is limited by representation of the explicit structures within the model. Without prior knowledge of the location and orientation of the $56^{o}/004^{o}$ release structure, modelling would not predict the observed behaviour.

Calibration of the south wall failure indicates that the rock mass strength required to match the measured and observed behaviour of the failure (GSI = 57.5) is less than the rock mass strength derived from drill hole and bench-face mapping (GSI = 60-70). This observation is consistent with the rock-mass scale effects reported by Hoek et al. (1995) and Sjöberg (1999) for the simulation of large-scale rock mass behaviour.

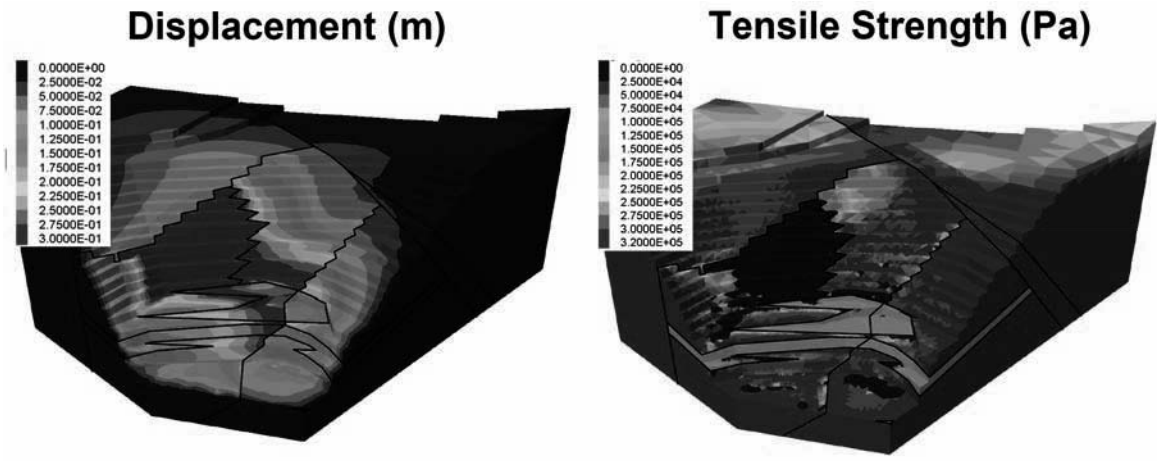

Figure 15 Slope displacement and reduction in tensile strength after mining of 445 RL bench (simulated combined worst-case rock mass, structure and phreatic surface conditions)

9 Conclusions

A calibration exercise has been conducted with the three-dimensional distinct element code *3DEC* to simulate the observed south wall failure at the Cadia Hill Pit. The numerical model provides a good correlation to the behaviour of the failure after mining of the 505 RL bench. Predictive analysis of the behaviour of the south wall after mining of the 445 RL bench indicates a minor increase in displacement and yielding in the area of the failure, but the extent of failure zone is predicted to remain confined to an approximate 60 m width between 625 RL and 535 RL, bounded by the original release structure.

The best-estimate rock mass model indicates a zone of increased displacement and yielding associated with the BE Fault zone on the 475 RL bench face, in the exact location as a 35,000 to 40,000 t failure that was triggered by significant rainfall runoff. Although the *3DEC* models analysed do not account for the pore pressures and increased rock mass density caused by significant rainfall surface runoff, analysis of the 475 RL bench failure highlights how a *3DEC* modelling approach can be used as a predictive tool to identify problem areas within the mining sequence.

Acknowledgements

The management of Newcrest Mining Limited, Cadia Valley Operations is acknowledged for permission to publish this paper.

References

Finn, D. (2006) Instability report south wall of the pit, Cadia Valley Operations Internal Memorandum.

Hajiabdolmajid, V. and Kaiser, P.K. (2002) Modelling slopes in brittle rock. NARMS-TAC 2002: Mining and Tunneling Innovation and Opportunity, Vol. 1, R. Hammah, W. Bawden, J. Curran, and M. Telesnicki (eds). Toronto: University of Toronto Press, pp. 331-338.

Hoek, E., Kaiser, P.K. and Bawden, W.F. (1995) Support of Underground Excavations in Hard Rock. Rotterdam: Balkema.

Itasca Consulting Group, Inc. (2007) 3DEC (Three-Dimensional Distinct Element Code), Version 4.02. Minneapolis.

Itasca Consulting Group, Inc. (2005) PFC2D (Particle Flow Code in Two-Dimensions), Version 3.1. Minneapolis.

Li, T. (2005) Geotechnical Engineering at Newcrest Mining, Australian Centre for Geomechanics Newsletter, Vol. 25.

Lowther, R. (2007) Geomechanical Instability Report – 475 RL Major Rainfall Triggered Rockfall Event, Cadia Valley Operations Internal Memorandum.

Sainsbury, D.P. and Urie, R. (2007) Stability Analysis of Horizontal and Vertical Paste Fill Exposures at the Raleigh Mine, Minefill 2007 – Innovation and Experience. Proceedings of the 9th International Symposium on Mining with Backfill, Montreal, May 2007, CD Proceedings, Paper No. 2527, CIM, Montreal.

Sjöberg, J. (1999) Analysis of Failure Mechanisms in High Rock Slopes, Doctoral Thesis, Department of Civil and Mining Engineering, Division of Rock Mechanics, Luleå University of Technology, 1999:01/ISSN: 1402-1544, January.